Rotor Fault Detection and Identification on Multicopter based on Statistical Data-driven Methods: Experimental Assessment via Flight Tests

Airin Dutta PhD Student
Jianxi Wang Undergraduate student
Fotis Kopsaftopoulos Assistant Professor
Farhan Gandhi Redfern Professor, Director

Center for Mobility with Vertical Lift (MOVE)
Rensselaer Polytechnic Institute, Troy, NY

ABSTRACT

A robust framework for fault detection and identification of rotor faults in multicopters is validated with data from experiments with a quadcopter and a hexacopter. The rotor fault detection and identification methods employed in this study are based on excitation-response signals of the aircraft under atmospheric disturbances. A concise overview of the development of the statistical time series model for healthy aircraft using the aircraft attitudes as the output and controller commands as the input is presented. This model is utilized to extract quality features for training a simple neural network to perform effective online rotor fault detection and identification. A proper justification of choosing the method of time-series assisted neural network has been given. It is shown a statistical time-series assisted neural network employed for online monitoring in the quadcopter and hexacopter achieves accuracy over 96% and 95%, respectively. It is effective under gusts and experimental variability encountered during outdoor flight and is sensitive to even partial loss of rotor thrust.

NOTATION

γ	:	Autocorrelation
τ	:	Lag
Σ	:	Residual covariance matrix
ARX	:	AutoRegressive with eXogenous excitation
BIC	:	Bayesian Information Criteria
CCF	:	Cross-Covariance Function
$E\{\cdot\}$	:	Expected value
FDI	:	Fault Detection and Identification
iid	:	identically independently distributed
IMU	:	Inertial Measurement Unit
LS	:	Least Squares
PE	:	Prediction Error
PSD	:	Power Spectral Density
RSS	:	Residual Sum of Squares
SPP	:	Samples Per Parameter
SPRT	:	Sequential Probability Ratio Test
SSS	:	Signal Sum of Squares
VAR	:	Vector AutoRegressive
NN	:	Neural Network
ML	:	Machine Learning
TSNN	:	Time-Series Assisted Neural Network

Presented at the Vertical Flight Society's 78th Annual Forum & Technology Display, Ft. Worth, Texas, USA, May 10–12, 2022.

INTRODUCTION

Advanced aerial mobility (AAM), fueled by the development of autonomous electric vertical take-off and landing (eVTOL) rotorcraft is set to revolutionize on-demand parcel delivery in major cities. According to a report by McKinsey Company, there will be 1.5 million drone deliveries in 2022 alone (Ref. 1). Given the highly constrained nature of such systems operating with a minimum of sensing and computational power, reliable fault detection and identification (FDI) of their components are critical. Actuator fault mid-air can create a safety hazard for persons in the surroundings. Thus it must be ensured that the drone is not only capable of detecting occurring failures but also of remaining airworthy and navigable at any time. Online information about system faults can facilitate safe landing through mitigating control and enable Condition Based Maintenance (CBM) via continuous monitoring of system faults. Therefore, the current research is driven toward realizing real-time system-level awareness and decision-making, utilizing in-flight data streams.

Multicopters have been identified as a potential platform for future AAM aircraft development due to their rotor redundancy, design flexibility, ability to integrate distributed electric propulsion, and their superior fault compensation capabilities. However, they exhibit strong non-linear dynamic coupling between rotors, structural components, fuselage, and control inputs, as well as time-varying cyclo-stationary behavior, and pose significant system identification and fault detection challenges when compared to fixed-wing aircraft. These issues have been addressed by (i) analytical model representations (Refs. 2–5), (ii) signal processing techniques (Refs. 6–10), and (iii) computational intelligence approaches (Refs. 11–18) – for a detailed review refer to Ref. 19. However, the available studies are either limited by analytical model building with the assumption of physical knowledge of the system available, arbitrary thresholds for detecting faults, or mostly concentrate on structural faults of blades, propellers, powertrain, etc. in rotorcraft. Some studies using data-driven methods are as follows. Ganguli *et al.* (Ref. 12) and Morel *et al.* (Ref. 11) employed neural networks (NN) to detect and trace faults and defects of helicopter rotor blades using noise-contaminated vibration data. Multicopter rotor structural damage detection and identification and has been demonstrated by Iannace *et al.* in Ref. 13 with acoustic signals and neural networks and by Bondrya *et al.* in Ref. 17 via support vector machines based on measurements of acceleration from the onboard IMU (Inertial Measurement Unit). Accurate blade fault detection and identification on a quadrotor using experimental airframe vibration signals were achieved with wavelet packet decomposition based features as input to a NN in Ref. (Ref. 18).

These limitations were collectively addressed by the authors via the use of stochastic time series representations of the multicopter dynamics based on flight signals (aircraft attitudes) without requiring knowledge of the system properties in Refs. 20–22. The rotor FDI approaches were developed within a statistical framework to account for operating and environmental uncertainty through properly defined statistical thresholds under predetermined confidence levels. Fast and accurate online rotor failure detection and identification on a hexacopter flying forward under different turbulence levels and uncertainty as well as varying forward velocity and gross weight were achieved (Refs. 20,21). Dutta *etal.* also proposed an innovative time-series assisted neural network (TSNN) for online rotor FDI followed by discrete quantification, wherein dynamically explainable features, acting as the input layer of the NN, were extracted from a statistical time-series model of the healthy aircraft. Its robust FDI performance under wind gusts with high accuracy and very small decision-making time was demonstrated in Refs. 23,24.

The objective of the present study is to experimentally validate the data-driven methods for early rotor FDI in multicopters developed in Refs. 20,23. Fault information in real-time can facilitate subsequent implementation of active fault tolerant control systems, planning alternative trajectories with limited control authority depending on the actuator fault severity, or reconfiguration of the vehicle to complete a safe flight in the event of rotor fault. This paper demonstrates the rotor fault detection and identification scheme on two aircraft, namely, the Parrot minidrone (quadcopter) and a self-built hexacopter. The data collection followed by the development of the data-driven methods have been discussed. It consists of two phases: the baseline training phase and the inspection phase. In the baseline phase, the input-output relationship of the healthy signals is represented by a stochastic time-series model, followed by training a machine-learning based algorithm to perform classification with the features extracted from the healthy model. This algorithm is a simple hidden layer neural network, which is termed time-series assisted neural network (TSNN). In the inspection phase, test signals have been filtered through the healthy model, and the residual crosscorrelation based feature input to the TSNN to detect and identify a rotor fault, simultaneously. The summary results show high accuracy with a few test sets, and an ablation study has also been performed to justify the need of the stochastic model along with a neural network.

Figure 1: Parrot Mambo Quadcopter ©Parrot Inc.

DATA GENERATION

Quadcopter

The Parrot Mambo Quadcopter shown in Fig. 1 is the main source of the flight data. The Parrot Minidrones Support from Simulink and Simulink Coder available in MATLAB is used for building the designed controller onto the hardware to command different flight maneuvers such as hover, forward flight, coordinated turns, etc., induce rotor faults of various magnitudes, and collect the in-flight sensor data streams.

The schematic of the flight controller in position control mode is designed as a PID-based control scheme with an outer and inner loop, shown in Fig. 2. The aircraft states are estimated via a combination of complementary and Kalman filters using the readings from the sensors mounted on the minidrone. The ultrasound sensor measures the distance of the minidrone above an object or surface and the pressure sensor measures the altitude. The camera with help of an image processing algorithm

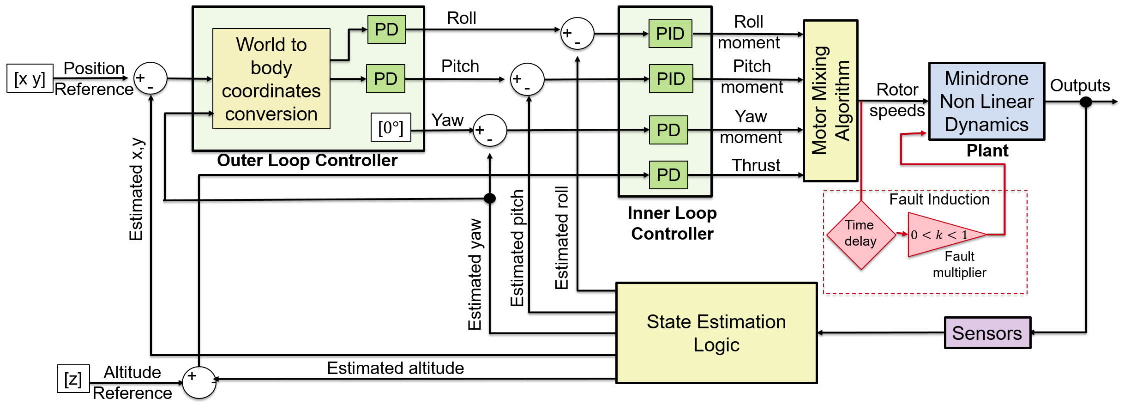

Figure 2: Controller Block and fault simulation in the minidrone

known as the optical flow determines the horizontal motion and speed of the aircraft. The Inertial Measurement Unit (IMU) contains a 3-axis accelerometer and a 3-axis gyroscope which measure the linear accelerations and the angular rates, respectively. After the controller outputs the required moments and thrust, the motor mixing matrix converts them into 4 commanded rotor speeds to be input to the plant. The aircraft dynamics block calculates the total forces and moments on the aircraft center of gravity and outputs the aircraft states. The forces and torques produced by the rotors are calculated assuming that they are proportional to the square of the rotor speeds, and are transformed from the rotor hub frame to the aircraft's center of gravity. The rotor in-plane forces are estimated as a fraction of rotor thrust based on a simplified blade element theory.

The raw signals coming from the sensors have been recorded during hover under healthy and degraded rotor conditions. These signals are corrupted by the sensor noise, disturbances, and uncertainty during flight experiments. A single front rotor degradation of 10 and 20 % is simulated by multiplying the controller commanded rotor speed with a factor of 0.9 and 0.8, respectively, at the time of commencement of the rotor fault. With no fault-tolerant controller in place, the minidrone crashes under higher degradation levels because the rotor speeds reach their saturation limit trying to compensate for the loss of thrust. The summary of the datasets obtained from flight experiments of the parrot minidrone is given in Table 1. Some of the datasets have been used in training phase, and the rest are reserved for testing the accuracy of the developed decision-making scheme.

Hexacopter

The self-designed Hexacopter shown in Fig. 3 is the primary source of the flight data. The aircraft's total weight,

Table 1: Summary of data from the Parrot minidrone

Number of datasets of		
Healthy	10% rotor fault	20% rotor fault
3*+13	3*+5	8

Sampling frequency= 200 Hz, Length of data = 15 s
* denotes training data

including the battery, is approximately 8.65 kg. The Hexacopter is constructed with the Tarot 680 Pro frame with a diameter of 695 mm, powered by MN3110 470KV motor from T-Motor with a 300 mm diameter propeller. The power of the Hexacopter is supplied by a 10,000 mAh 6S battery with a 30C discharge rate, enabling the aircraft to hover at around 40 percent throttle. The Hexacopter dynamics are controlled by a Cube Orange Pixhawk flight controller with Ardupilot firmware. The Hexacopter has three IMUs onboard, two from the flight controller and one from the Here3 Global Positioning System (GPS); combined, they provide three sets of IMU data on all 6 degrees of freedom, measuring the linear acceleration and angular acceleration, respectively. The integrated flight controller log collects data on all signals, such as the radio controller input and Electronic Speed Controller (ESC) output.

A clockwise rotating faulty propeller shown in Fig. 4 is used to simulate a thrust degradation due to structural failure. The faulty propeller has a symmetrical surface area lost at the tip, a 16.67% decrease in propeller diameter. The faulty propeller was mounted at motor position 3, 1, and 6 as shown in Fig. 5 to simulate the front, side, and back rotor fault. Data were collected with aircraft hovering at a steady-state outdoor in an uncontrolled environment, the aircraft is subjected to unpredictable external force due to wind in all directions. The position and altitude of hover are varied randomly in between steady flights to capture maximum experimental variability in the data. During the data collection phase of each flight,

Figure 3: Hexacopter with considered rotor faults

the aircraft was hovering under Loiter mode. Under Loiter mode, the flight controller passes the internal IMU data and GPS data through the Extended Kalman Filter (EKF) to generate an estimated relative altitude and position. The target altitude and position are then passed to the control system, generating a Pulse Width Modulated (PWM) control output to ESCs accordingly (Ref. 25). The summary of the datasets generated from the hexacopter is given in Table 2.

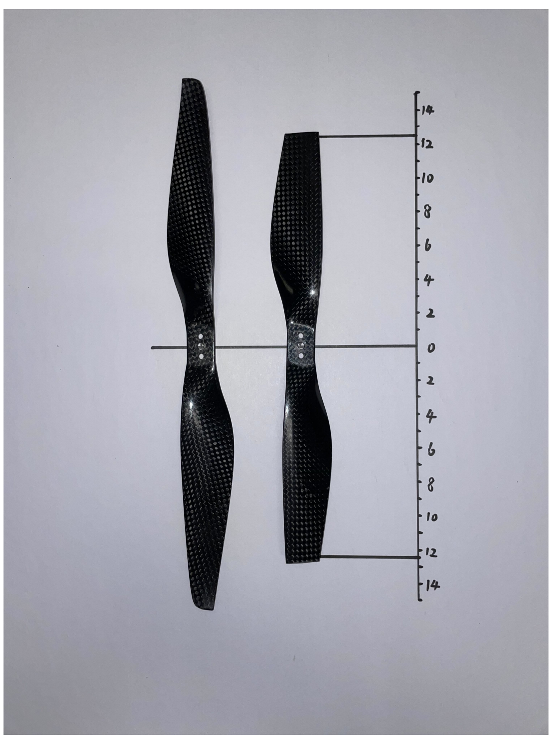

Figure 4: Healthy and faulty propeller

Table 2: Summary of data from hexacopter

Health state	Number of datasets
Healthy	2*+1
Front rotor fault	10*+5
Side rotor fault	10*+5
Back rotor fault	10*+5

Sampling frequency= 10 Hz, Length of data = 60 s
* denotes training data

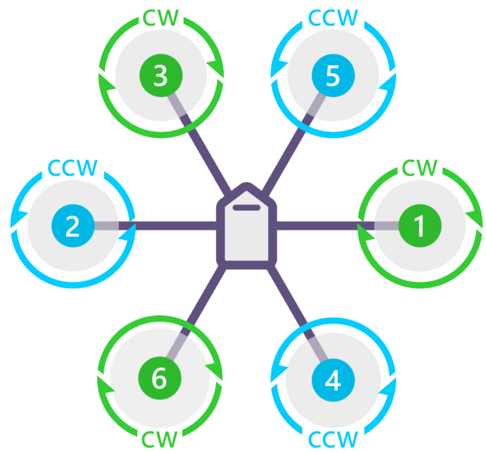

Figure 5: Hexacopter X-configuration

METHODOLOGY

General Workframe of Rotor Fault Detection and Identification

Let Z_o be signals that designate the aircraft under consideration in its healthy state, and Z_1, Z_2 and Z_6 the aircraft under fault of Rotor 1,2, and 6. Z_u designates the unknown (to be determined) state of the aircraft. Statistical learning methods explored in this study are based on discretized aircraft states signals $y[t]$ [1] and control signals $u[t]$ (for $t = 1,2,\ldots,N$). Here, N denotes the number of samples, and the conversion from discrete normalized time to analog time is based on $(t-1)T_s$, with T_s being the sampling period. The signals are represented by Z and subscript $(o,1,2,6,u)$ is used to denote the corresponding state of the aircraft that produced the signals.

The signals generated from simulation can be analyzed by parametric or non-parametric statistical methods and proper models are fitted and validated. Such models are trained for the cases Z_o, Z_1, Z_2, Z_6 in the baseline phase. Fault detection and identification is performed in the online inspection phase with the information extracted from the current unknown signals with the baseline models, de-

[1] A functional argument in parentheses designates function of a real variable; for instance $x(t)$ is a function of analog time $t \in \mathbb{R}$. A functional argument in brackets designates function of an integer variable; for instance $x[t]$ is a function of normalized discrete time $(t = 1,2,\ldots)$.

signing decision-making scheme based on statistical hypothesis testing or machine learning (ML) based classification algorithm.

However, in the presence of transient disturbances such as gusts, which are commonly encountered during flight causes increased false alarms with statistical decision-making (Ref. 20). To this end, an innovative approach was developed by the authors to utilize ML based classification algorithm along with the statistical time-series representation of the dynamics of the signals obtained from a hexacopter. This method, titled as the time-series neural network (TSNN) is described in Refs. 23, 24. Neural Networks are excellent classifiers, able to accommodate noise and uncertainty in data with carefully chosen features and regularization parameters making it attractive for our application, where the aim is to develop a robust rotor FDI framework with signals affected by atmospheric disturbances encountered in real flight. But often these ML techniques focus on fitting the data and suffer from a lack of explainability. Therefore, the focus was to develop interpretable features that extract important dynamic information from the aircraft signals, to be input to a single hidden layer NN that only serves as a single-step classifier tool. these features are extracted with the help of a statistical time-series model since it can represent the dynamics of the system. This study validates the developed framework, as shown in Fig. 6 with data generated from flight experiments on 2 types of multicopters, namely, a quadcopter and a hexacopter.

Vector ARX Model Identification for Healthy Aircraft

Vector AutoRegressive (VARX) models employ multi-dimensional signals, i.e. m-dimensional aircraft attitudes as the response and n-dimensional control signals as excitation, for input-output time series modeling (Refs. 26, 27) given by:

$$\mathbf{y}[t] = \sum_{i=1}^{na} \mathbf{A}_i \cdot \mathbf{y}[t-i] + \sum_{i=0}^{nb} \mathbf{B}_i \cdot u[t-i-nk] + \mathbf{e}[t]$$
$$\text{with} \quad \mathbf{e}[t] \sim \text{iid}\,\mathcal{N}(\mathbf{0}, \boldsymbol{\Sigma}), \quad \boldsymbol{\Sigma} = E\{\mathbf{e}[t] \cdot \mathbf{e}^T[t]\} \tag{1}$$

with $\mathbf{A}_i$ $(m \times m)$ designating the i-th AR matrix, $\mathbf{B}_i$ $(m \times n)$ designating the i-th X matrix, $\mathbf{e}[t]$ $(m \times 1)$ the model residual sequence characterized by the non-singular and generally non-diagonal covariance matrix $\boldsymbol{\Sigma}$, na the AR order, nb the X order, nk the delay in terms of lag between response and input signals and $E\{\cdot\}$ statistical expectation. Given the attitude signal measurements $y[t]$ $(t = 1, 2, \dots, N)$, the estimation of the VARX parameter vector $\boldsymbol{\theta}$ comprising all AR and X matrix elements ($\boldsymbol{\theta} = \text{vec}([\mathbf{A}_1 \quad \mathbf{A}_2 \dots \mathbf{A}_{na} \quad \mathbf{B}_0 \quad \mathbf{B}_1 \dots \mathbf{B}_{nb}])$ and the residual covariance matrix $\boldsymbol{\Sigma}$ is accomplished via linear regression schemes based on minimization of the Ordinary Least Squares (OLS) or the Weighted Least Squares (WLS) criterion (Refs. 28, 29). The modeling procedure involves the successive fitting of VARX(na, nb, nk) models while sweeping through increasing AR and X orders, na and nb respectively and delay, nk, until an adequate model is achieved. The model order is chosen by minimum Bayesian Information Criteria (BIC) and Residual sum of Squares over Signal Sum of Squares Criterion (RSS/SSS) criteria (Ref. 30) given by the following equations:

$$BIC = \ln\left(trace(\boldsymbol{\Sigma})\right) + (d \times \ln N)/N \tag{2}$$

$$RSS/SSS = \sum_{i=1}^{m} \frac{\sum e_i^2}{\sum y_i[t]^2} \qquad \forall \quad t = 0, 1, ..., N \tag{3}$$

where, d denotes the number of free parameters estimated for the VARX model and N denotes the number of samples used for estimation. BIC is a statistical criterion that penalizes model complexity (order, and hence the number of free parameters) as a counteraction to a decreasing model fit criterion. RSS/SSS criteria determines the predictive capability of the model.

Time-Series Assisted Neural Network

The VARX model for healthy aircraft is used to filter the aircraft signals (response and controls) and obtain output residuals. Important information about the dynamics of the aircraft is embedded in the output residuals and controller commands due to the incorporation of a feedback controller. To this effect, crosscorrelation between the output residuals and inputs have been identified as a powerful feature to distinguish between different rotor faults and gust affected healthy flight.

The crosscorrelation function between two signals $z(t)$ and $x(t)$, denoted by $\gamma_{zx}[\tau]$ is given by Eq. 4.

$$\gamma_{zx}[\tau] = E\{z[t] \cdot x[t+\tau]\} \tag{4}$$

where τ is the time lag in number of samples.

The crosscorrelation function is fed to the input layer of a 2-layer NN to classify 4 classes: healthy flight and front, side, and back rotor faults.

The input layer is denoted by $\mathbf{x}^T$ and the output layer is denoted by $\mathbf{h}(\mathbf{x})$ and is related by the following equation:

$$\mathbf{h}(\mathbf{x}) = \theta\left(\mathbf{W_2}^T\left(\theta\left(\mathbf{W_1}^T\mathbf{x}\right) + \mathbf{B_1}\right) + \mathbf{B_2}\right) \tag{5}$$

where, $\theta(s)$ indicates the hyperbolic tangent activation function given by $\theta(s) = \dfrac{e^s - e^{-s}}{e^s + e^{-s}}$. The weight matrices and bias vectors for the two layers denoted by

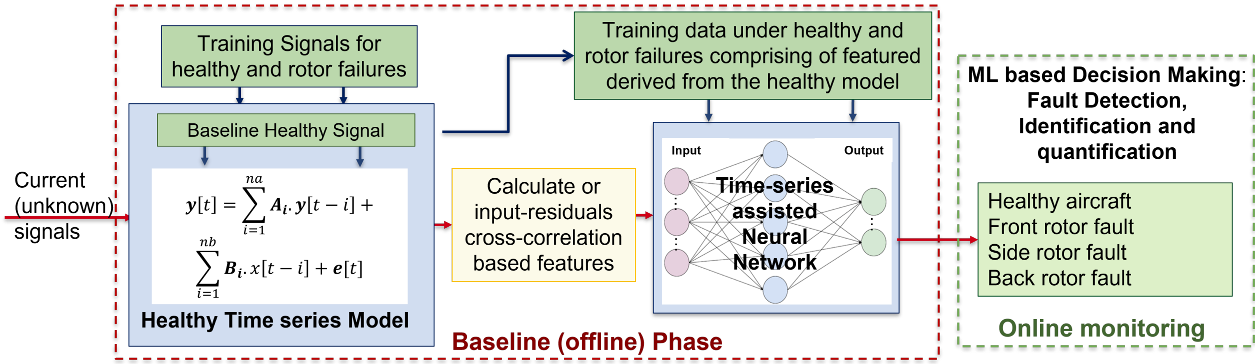

Figure 6: General workframe of time-series neural networks

$\mathbf{W_1}, \mathbf{W_2}$ and $\mathbf{B_1}, \mathbf{B_2}$ are determined in the baseline training phase by backpropagation learning techniques to minimize classification error.

RESULTS FOR QUADCOPTER

Signals

The minidrone was flown repeatedly in outdoor and indoor conditions under hover for over 8 days to capture experimental variability in flight. Figures 7a and 7b show the time history of the IMU and controller command signals collected from a Parrot Mambo minidrone commanded to hover at a height of 1.1 m off the ground. In the data sets collected, a front rotor fault occurs at $t = 20$ s, indicated by the vertical black dashed line. Fig. 7a represent 10 and Fig. 7b represent 20% rotor fault. The aircraft takes about 3 seconds to take off before settling onto a steady hover, evident from the angular rates signals. Therefore, the steady-state signals from 5-10 s have been used as healthy signals. Immediately after the rotor fault commencement, the signals show a transient response due to the sudden loss in thrust in the faulty rotor, as observed from the marked change of variance of the angular rate signals. The controller compensates for the fault by increasing the commanded rotor speed to the faulty rotor and the flight achieves a steady-state within 10 s. In the following analysis, the rotor degradation signals are considered as the fault-compensated steady-state signals from 30-45 s, shown in Figs. 7a and 7b. It can be observed from the bottom plots that the faulty rotor speed is quickly compensated for and the mean of the speed outputs are similar in healthy and faulty rotor states. To this end, this method relies on capturing the input-output dynamics of the system, properly represented by statistical time-series models.

Model identification and neural network training

Vector (multi-variate) parametric identification of the aircraft dynamics has been based on 15 s ($N = 3000$ samples at a sampling frequency of 200 Hz) of aircraft angular rates and control signals obtained from healthy aircraft flight under hover. In the present case, the response comprises the roll, pitch, and yaw rates and the excitation are the 4 independent rotor speeds. The model parameters and model order, A_i, B_i and na, nb, nk, respectively (Eq. 1), need to be estimated so that the model properly represents the dynamics of the system under healthy conditions. The modeling strategy consists of successive fitting of VAR(na, nb, nk) models until a suitable model with the least amount of complexity (number of parameters) and best fit is selected, as shown in Fig. 8a.

Model order selection is based on a combination of Bayesian Information Criteria (BIC) (Eq. 2) and Residual sum of squares normalized by Signal sum of squares (RSS/SSS) criteria (Eq. 3). A model order of $na = 12, nb = 12, nk = 0$ yields the minimum BIC and this model is represented as VARX$(12,12,0)$. This order exhibits a very low RSS/SSS value of 0.14% demonstrating accurate identification and excellent dynamics representation of the healthy aircraft under hover. The number of parameters estimated for the VARX$(12,12,0)$ model is 252, which results in a Samples per Parameter (SPP) ratio of 83.33 ($\frac{N}{d}$), and the suggested value is more than 15 (Ref. 31).

The model was validated based on the fact that the model matching the current state of the system should generate output residual sequences which are uncorrelated. Consequently, using a healthy aircraft signal that has been generated from a different flight experiment, it has been seen that the crosscorrelation function of the output residual sequences obtained from the healthy model has been observed to be more or less white with 95% confidence, as shown Fig. 8b (confidence intervals shown in blue).

From Ref. 23, it has been observed that crosscorrela-

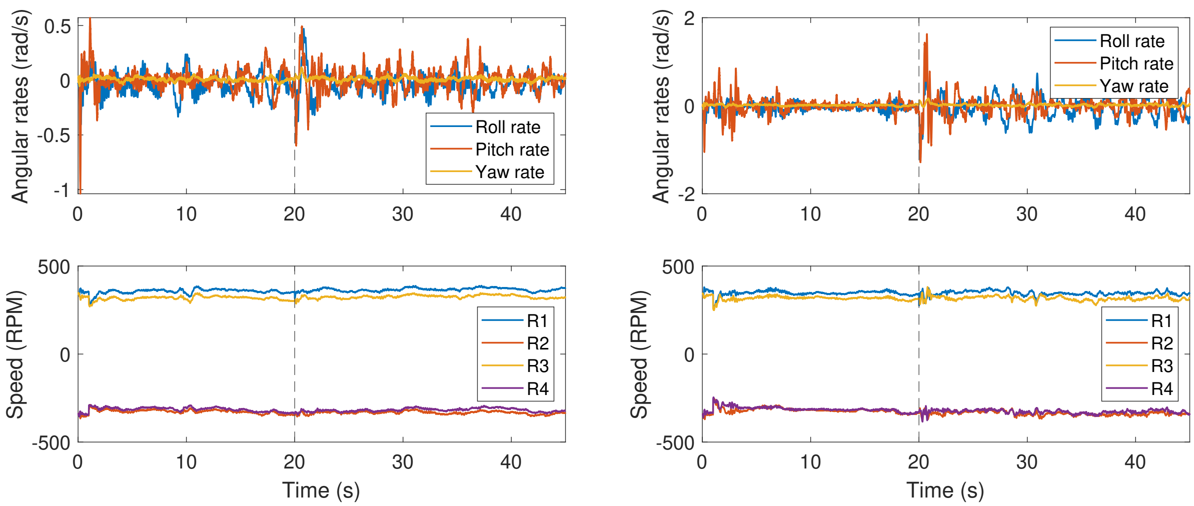

(a) 10% rotor degradation

(b) 20% rotor degradation

Figure 7: Time history of IMU and rotor command signals from Parrot Minidrone under hover. The vertical black dashed line indicates the instant of rotor fault commencement.

tion of output residuals, obtained via a statistical model of a healthy aircraft, has better capability to detect and identify rotor failures using simple NN than signals only. Crosscorrelation function serves as a "good" feature for fault classification. To this end, output residuals and input signals (controller commands) have been obtained from filtering the different healthy and faulty signals of 1 s length through the healthy aircraft model. Next, the crosscorrelation of these with each other up to a positive lag of 20 is fed through the first layer of the NN. The first classification consists of healthy signals. The rotor fault class has been trained with only signals with 10% degradation. Therefore, this network, having output classes as healthy aircraft and faulty, can only detect rotor faults. Note that the number of training data sets (See Table 1) should be balanced for the different classes to avoid classifier bias. The details of this TSNN are given in Table 3. Note that the training method has been used as the Bayesian regularization because of the limited number of datasets available.

Rotor Fault Detection and Identification results

Aircraft attitude rates and rotor speeds signals obtained from the current flight of minidrone, with window length 1 s updated every 1 s, are filtered through the identified healthy time series model, followed by the crosscorrelation between inputs and output residuals being driven through the trained network. Indicative fault monitoring results are shown in Fig. 9. The top plot shows healthy flight and the bottom plot shows fault-compensated flight with 20% rotor fault. Note that these datasets have not been used in the training phase. The markers 'o' and '+' denotes healthy and faulty flight respectively. The decision is mostly accurate, with one false alarm during the healthy flight.

Table 3: Time-Series assisted neural network training for the Parrot minidrone

Input Type	Crosscorrelation between output residuals and input signals (1 s)
Input Layer Size	1029
Training Function	Bayesian regularization backpropagation
Hidden Layer Size	8
Output	2 (Healthy and rotor faults)
Cost Function	Mean-squared error
Activation Function	Hyperbolic Tangent Function
Performance	4.33×10^{-6}

Table 4: Fault detection results for time-series assisted neural network on the Parrot minidrone

False Alarms	Missed faults
9.63	0

All the metrics are given in percentages

The summary results for fault detection calculated from the test data given in Table 1 are given in Table 4. It shows a total accuracy of 96%, with some false alarms but no missed faults. Note that the metrics are shown in percentages, as multiple decisions are made throughout the flight time in a single data set. Since only a single type of rotor fault with varying severity is considered in

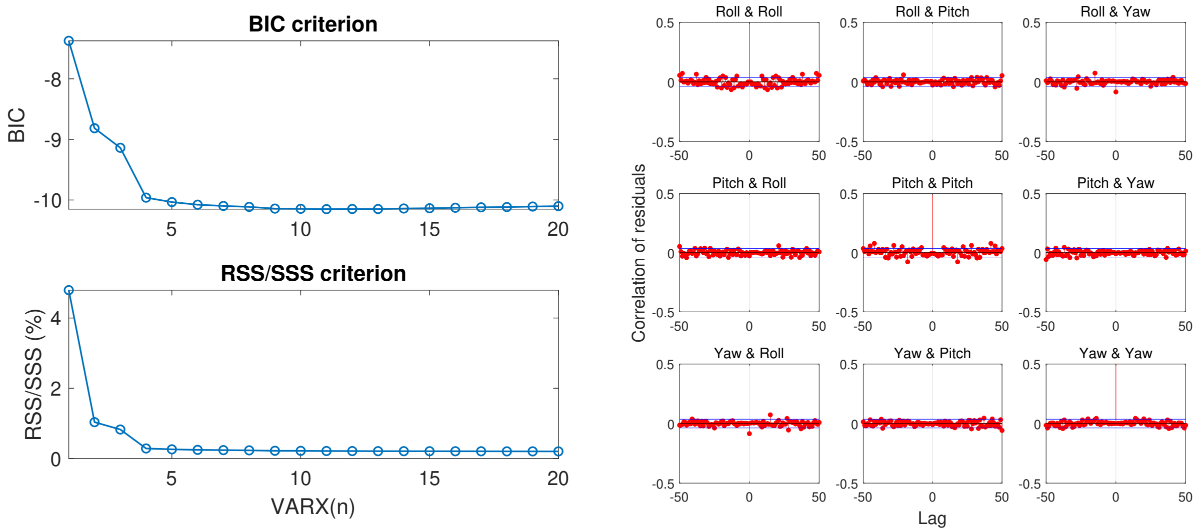

(a) Model selection

(b) Model validation

Figure 8: Model identification for healthy hover of the Parrot Minidrone

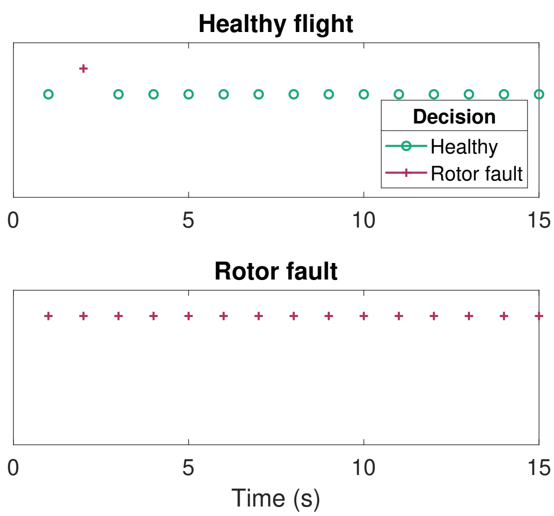

Figure 9: Online monitoring results for the Parrot minidrone

this case, there is no data for calculating a fault confusion matrix.

RESULTS FOR HEXACOPTER

Signals

The lab-built hexacopter flight experiments were conducted outdoors only over 6 days under varying levels of windy weather. Figures 10 and 11 show the indicative flight signals obtained under healthy and front rotor faults, respectively. The top subplots show the estimated values of the roll, pitch, and yaw attitudes, and the bottom plots the estimated individual rotor speeds, respectively. Note that the output signals have been mean-compensated due to the difference in yaw command in different flights. All the signals are stochastic in nature due to both the atmospheric disturbances, as well as the sensor noise. The roll and pitch should have a statistical mean zero, since a hover is commanded. It can be observed that the variances of the signals in front rotor faults are higher than that in healthy flight. However, that can be contributed to the change in weather conditions under which the flight tests were conducted. The power spectral density of the output signals show little difference in the dynamic content, due to the fact that the loss of rotor thrust due to fault was compensated by increasing the rotor speeds. Therefore, the relationship between the rotor speeds along with the attitudes needs to be captured to determine the rotor faults. Indicative signals for side and back rotor fault has been shown in the Appendix, Figs. 16 and 17, respectively.

Model identification and neural network training

Vector (multi-variate) parametric identification of the aircraft dynamics has been based on 15 s ($N = 600$ samples at a sampling frequency of 10 Hz) of aircraft attitudes and individual rotor speeds obtained from healthy hexacopter flight under hover. In the present case, the response consists of the roll, pitch, and yaw rates and the input signals are the 6 independent rotor speeds. The model parameters and model order, A_i, B_i and na, nb, nk, respectively (Eq. 1), are estimated so that the model properly represents the dynamics of the system under healthy conditions. Similar to the exercise with minidrone, the $\mathrm{VAR}(na, nb, nk)$ model is estimated by the weighted least

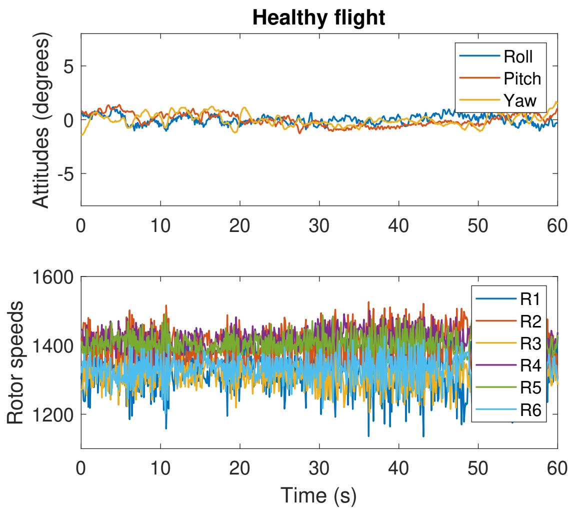

Figure 10: Healthy flight

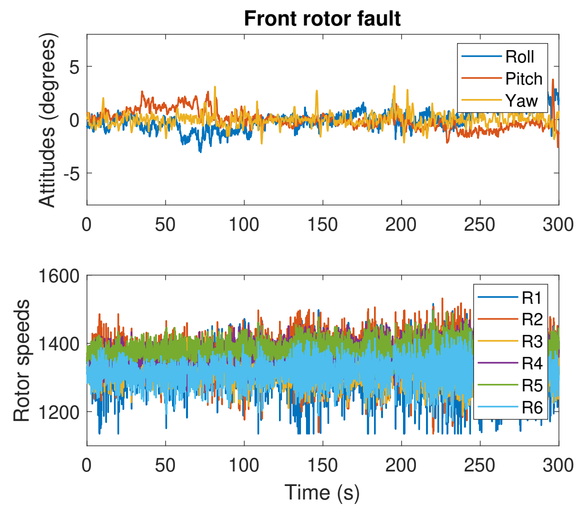

Figure 11: Front rotor fault

Figure 12: Time history of attitudes and rotor speeds from the hexacopter under steady hover

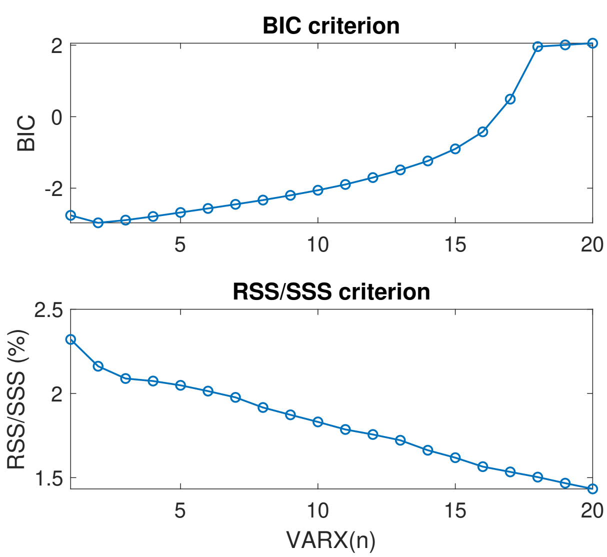

Figure 13: Model selection for healthy flight of the hexacopter

squares approach, and the model order is selected by Bayesian Information Criteria (BIC) (Eq. 2) and the Residual sum of squares normalized by Signal sum of squares (RSS/SSS) criteria (Eq. 3), as shown in Fig. 13. A model order of $na = 2, nb = 2, nk = 0$ yields the minimum BIC. However, the model order is chosen as $na = 2, nb = 2, nk = 0$, by examining the whiteness of the residuals as shown in Fig. 14a and this model is represented as VARX$(3,3,0)$. This order exhibits an RSS/SSS value of 2.08% which is sufficient given that there were gusts affecting the flight under hover. The number of parameters estimated for the VARX$(3,3,0)$ model is 81, which results in a Samples per Parameter (SPP) ratio of 66.66 $(\frac{N}{d})$.

The model was validated based on the fact that the model matching the current state of the system should generate output residual sequences which are uncorrelated with each other as well as the input signals. Consequently, a healthy aircraft signal has been generated from a different flight experiment. The crosscorrelation function of the output residual sequences obtained from driving the current signals from a healthy aircraft through the healthy model has been observed to be white with 95% confidence, as shown Fig. 14a (confidence intervals shown in blue). Next, the crosscorrelation function of residuals obtained from driving the degraded front rotor flight signals through the identified healthy model has been presented in Fig. 14b. It shows that the residual sequences are correlated as they exceed the confidence limits for most of the lags. This denotes that the input-output relationship represented by the healthy model changes due to a rotor fault. This information has been crucial for designing ML based classifiers to detect and identify rotor faults (Ref. 23).

Similarly, for fault detection and identification in the hexacopter, a TSNN is trained with the crosscorrelation of output residuals and input signals (controller commands) obtained from filtering the different healthy and faulty signals of 10s length through the healthy aircraft model. The crosscorrelations are considered up to a positive of 5 and serve as the first layer of the TSNN. The output classes of this network are healthy flight, front rotor fault, back rotor fault, and side rotor fault, trained with 10 sets of training datasets each, as per Table 2. The other details of training this network are given in Table 5. Note that the training method has been used as the Bayesian

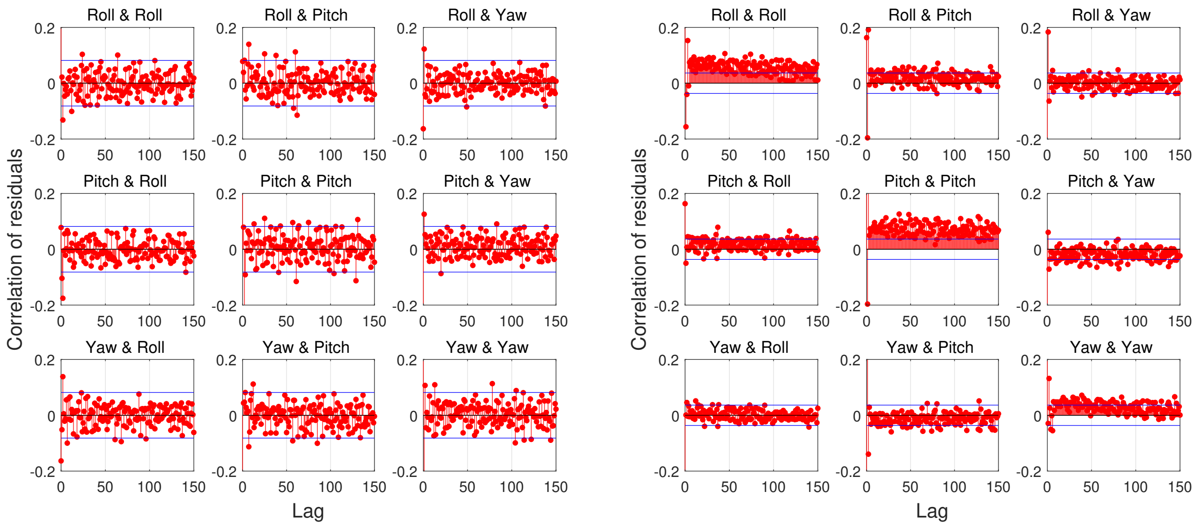

(a) Signals from healthy flight

(b) Signals from front rotor fault

Figure 14: Crosscorrelations of the residuals obtained from the healthy model of the hexacopter

Table 5: Time-series assisted neural network training for the hexacopter

Input Type	Crosscorrelation between output residuals and input signals (10 s)
Input Layer Size	486
Training Function	Bayesian regularization backpropagation
Hidden Layer Size	2
Output classes	4 (Healthy and front, side, and back rotor faults)
Cost Function	Mean-squared error
Activation Function	Hyperbolic Tangent Function
Performance	9.31×10^{-10}

regularization as it negates the need for a validation data set.

Rotor Fault Detection and Identification results

Aircraft attitudes and individual rotor speeds signals obtained from the current flight of the hexacopter, with window length 10 s updated every 1 s, are driven through the identified healthy time series model. The crosscorrelation between inputs and output residuals is fed through the trained network, which performs fault detection and identification simultaneously. Indicative fault monitoring results are shown in Fig. 15. The title of the figure denotes the health condition under which the signals being monitored are obtained. These signals are test signals denoted in Table. 2, and are not used in the training phase. The markers '+', '*', 'o', and 'x' denotes healthy, front rotor fault, side rotor fault, and back rotor fault decisions, respectively. The decisions shown in these indicative signals in Fig. 15 are mostly accurate.

Table 6: Fault detection and identification results with time-series assisted neural network for the hexacopter

(a) Fault detection

False Alarms	Missed faults for faults of		
for Healthy flight	Front rotor	Side rotor	Back rotor
6.87	0	0	0

(b) Fault classification confusion matrix

Decision	Signals for		
	Front rotor	Side rotor	Back rotor
Front rotor	100	0	0
Side rotor	0	91.11	8.89
Back rotor	0	2.75	97.25

All the metrics are given in percentages

The summary results for fault detection and identification calculated from the test data given in Table 2 are given in Tables 6a and 6b, respectively. Table 6a shows a fault detection accuracy of 93%, with 7% false alarms and no missed faults. The fault identification is mostly accurate, with some confusion between the side and back rotor faults. The accuracy metrics are shown as the percentage of the accurate decisions made throughout the flight time. Note, in calculating false alarms, the type of fault denoted by the wrong decision is irrelevant, hence it is shown separately from the confusion matrices with other faults. Due to this fact, the rows of the fault identification confusion matrices may not add up to 100% when there are missed faults present.

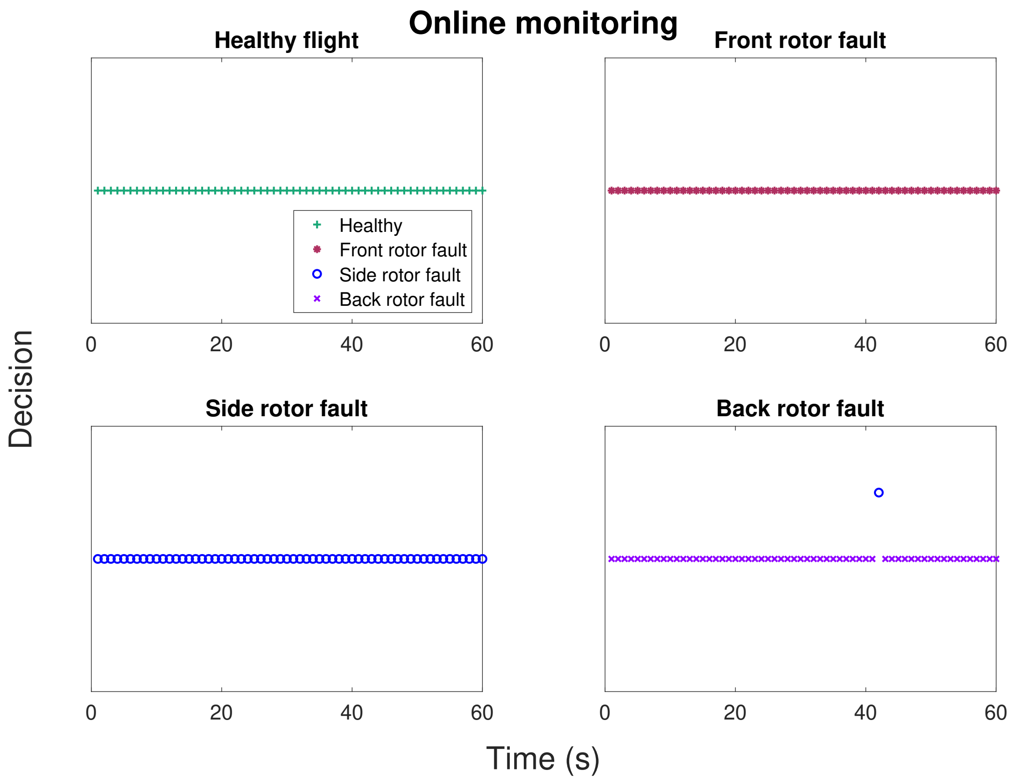

Figure 15: Online monitoring results for the hexacopter

Table 7: Fault detection and identification results with the signal crosscorrelation neural network (ablation study) for the hexacopter

(a) Fault detection

False Alarms	Missed faults for faults of		
for Healthy flight	Front rotor	Side rotor	Back rotor
0	30.93	1.03	1.07

(b) Fault classification confusion matrix

Decision	Signals for faults of		
	Front rotor	Side rotor	Back rotor
Front rotor	69.07	0	0
Side rotor	0	98.27	0.7
Back rotor	2.37	16.15	80.41

All the metrics are given in percentages

It is important to perform an ablation study here, to ascertain the significance of the time-series model in the data-driven decision-making scheme. In machine learning applications, an ablation study is a set of experiments in which components of a machine learning system are removed or replaced in order to measure the impact of these components on the performance of the system. This helps justify the inclusion of the important components or removal of certain components that do not improve the performance to reduce the complexity. Therefore in this application, a NN has been trained with the signal cross-correlations only, eliminating the time-series representation of the healthy dynamics. The size of the input layer, i.e. the number of lags considered in the crosscorrelation and the hidden layer size has been kept the same as the TSNN described in Table 5. Also, the same training and test data have been considered to evaluate and contrast the performance of the two schemes. The summary results for the study is given in Tables 7a and 7b. It has shown an overall accuracy of 79.64%, which is much lower than that obtained with the TSNN. There are more false alarms, especially with the front rotor fault and the confusion between the rotor faults also increases due to elimination of the time-series model.

CONCLUSIONS

This paper provides experimental validation for statistical time-series assisted data-driven methods to detect and classify rotor faults in multicopters under atmospheric disturbances and uncertainty. Development of statistical time series models (response only and input-output) to represent healthy aircraft dynamics has been discussed followed by the development of machine-learning based fault detection and identification methods assisted by information obtained from the model estimated from the healthy aircraft. The important conclusions from the study are summarized below.

- Stochastic methods for rotor fault detection and identification in multicopters achieve effective decision making based on (i) aircraft state and control signals, (ii) statistical model building, and (iii) machine-learning algorithms.
- The knowledge of controller effort can be used along with the aircraft output to detect and classify the rotor faults.
- The crosscorrelation function between input signals and output residuals obtained from an input-output statistical model for healthy aircraft serves as a powerful feature for classification with a machine learning algorithm.
- With the right feature, which is the crosscorrelation function of signals obtained from various health conditions, even a simple single hidden-layer neural network is capable of detecting and identifying rotor faults.
- In the online phase, the time-series assisted neural network has been shown to achieve fault detection and identification accuracy of over 95%.
- An ablation study, eliminating the stochastic time-series representation shows that the signals cross-correlations are not as good features as the residual crosscorrelations, resulting in high false alarms and fault misclassification with the neural network.
- In the future, more flights regimes such as hover, forward flight, and coordinated turns will be included with more rotor fault scenarios comprising of types and magnitude of rotor faults.

APPENDIX

Figures 16 and 17 show the indicative flight signals obtained from the hexacopter under side, and back rotor faults, respectively.

REFERENCES

1. "Drone delivery: More lift than you think," [Online; accessed 4-February-2022].
2. "System Identification Modeling of a Small-Scale Unmanned Rotorcraft for Flight Control Design," Vol. 47, (1), January 2002, pp. 50–63. DOI: /10.4050/JAHS.47.50
3. Freddi, A., Longhi, S., Monteriù, A., and Prist, M., "Actuator Fault Detection and Isolation System for an Hexacopter," IEEE/ASME 10th International Conference on Mechatronic and Embedded Systems and Applications, August 2014. DOI: 10.1109/MESA.2014.6935563
4. Serafini, J., Bernardini, G., Porcelli, R., and Masarati, P., "In-flight health monitoring of helicopter blades via differential analysis," *Aerospace Science and Technology*, Vol. 88, 2019, pp. 436–443. DOI: https://doi.org/10.1016/j.ast.2019.03.039
5. Ghalamchi, B., Jia, Z., and Mueller, M. W., "Real-Time Vibration-Based Propeller Fault Diagnosis for Multicopters," *IEEE/ASME Transactions on Mechatronics*, Vol. 25, (1), 2020, pp. 395–405. DOI: 10.1109/TMECH.2019.2947250
6. Waschburger, R., Paiva, H. M., e Silva, J. J. R., and Galvão, R. K. H., "Fault detection in a laboratory helicopter employing a wavelet-based analytical redundancy approach," Conference on Control and Fault-Tolerant Systems, Nice, France, 2010.
7. Schwartz, B. C., and Jones, D. L., "Quadratic and instantaneous frequency analysis of helicopter gearbox faults," *Mechanical Systems and Signal Processing*, Vol. 14, (4), 2000, pp. 579–595.
8. Williams, W. J., and Zalubas, E. J., "Helicopter transmission fault detection via time-frequency, scale and spectral methods," *Mechanical Systems and Signal Processing*, Vol. 14, (4), 2000, pp. 545–559.
9. Cox, J. R., Arnold, S., and Anusonti-Inthra, P., "Rotor Blade Fault Detection through Statistical Analysis of Stationary Component Vibration," 52nd AIAA/SAE/ASEE Joint Propulsion Conference, July 2016. DOI: 10.2514/6.2016-4642
10. Lu, F., Li, Z., Huang, J., and Jia, M., "Hybrid State Estimation for Aircraft Engine Anomaly Detection and Fault Accommodation," *AIAA Journal*, Vol. 58, (4), 2020, pp. 1748–1762. DOI: 10.2514/1.J059044
11. Morel, H., Ouladsine, M., Krysinski, T., and Brun-Picard, D., "Defect detection and tracing on helicopter rotors by artificial neural networks," IEEE Advanced Process Control Applications for Industry Workshop, Vancouver, Canada, 2005.
12. Ganguli, R., Chopra, I., and Haas, D. J., "Helicopter Rotor System Fault Detection Using Physics-Based Model and Neural Networks," *AIAA Journal*, Vol. 36, (6), May 1998, pp. 1078–1086.

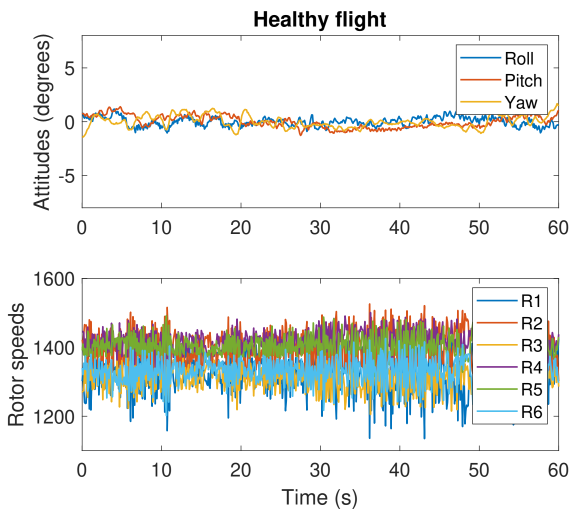

Figure 16: Side rotor fault

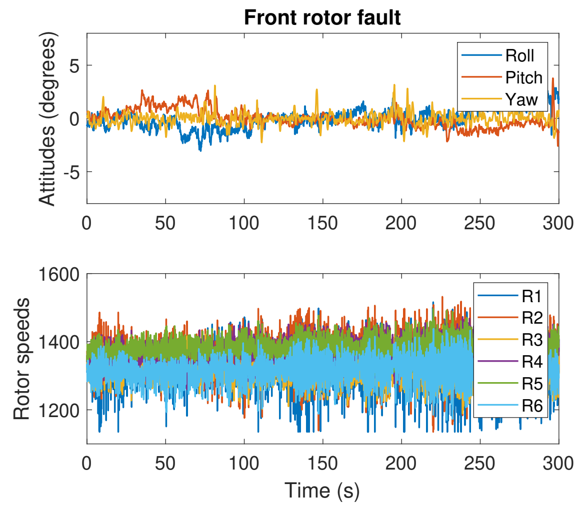

Figure 17: Back rotor fault

Figure 18: Time history of attitudes and rotor speeds from the hexacopter under steady hover

13. Gino Iannace, G. C., and Trematerra, A., "Fault Diagnosis for UAV Blades Using Artificial Neural Network," *Robotics*, Vol. 8, (3), 2019. DOI: 10.3390/robotics8030059

14. Ganguli, R., "Health Monitoring of a Helicopter Rotor in Forward Flight Using Fuzzy Logic," *AIAA Journal*, Vol. 40, (12), December 2002.

15. Ochoa, C. A., and Atkins, E. M., "Multicopter Failure Diagnosis through Supervised Learning and Statistical Trajectory Prediction," 2018 AIAA Information Systems-AIAA Infotech @ Aerospace, Kissimmee, Florida, January 2018.

16. Baskaya, E., Bronz, M., and Delahaye, D., "Fault detection diagnosis for small UAVs via machine learning," 2017 IEEE/AIAA 36th Digital Avionics Systems Conference (DASC), 2017.

17. Bondyra, A., Gasior, P., Gardecki, S., and Kasiński, A., "Fault diagnosis and condition monitoring of UAV rotor using signal processing," , 09 2017. DOI: 10.23919/SPA.2017.8166870

18. Jiang, Y., Zhiyao, Z., Haoxiang, L., and Quan, Q., "Fault detection and identification for quadrotor based on airframe vibration signals: A data-driven method," 2015 34th Chinese Control Conference (CCC), 2015. DOI: 10.1109/ChiCC.2015.7260639

19. Qi, X., Theillol, D., Qi, J., Zhang, Y., and Han, J., "A Literature Review on Fault Diagnosis Methods for Manned and Unmanned Helicopters," 2013 International Conference on Unmanned Aircraft Systems, May 2013.

20. Dutta, A., McKay, M., Kopsaftopoulos, F., and Gandhi, F., "Statistical residual-based time series methods for multicopter fault detection and identification," *Aerospace Science and Technology*, Vol. 112, 2021, pp. 106649. DOI: https://doi.org/10.1016/j.ast.2021.106649

21. Dutta, A., McKay, M., Kopsaftopoulos, F., and Gandhi, F., "Rotor Fault Detection and Identification on a Hexacopter under Varying Flight States Based on Global Stochastic Models," Vertical Flight Society 76th Annual Forum, Online (due to COVID-19), October 2020.

22. Dutta, A., Niemiec, R., Kopsaftopoulos, F., and Gandhi, F., "Unified Statistical Framework for Rotor Fault Diagnosis on a Hexacopter via Functionally Pooled Stochastic Models," Vertical Flight Society 77th Annual Forum, Online (due to COVID-19), May 2021.

23. Dutta, A., McKay, M. E., Kopsaftopoulos, F., and Gandhi, F., "Multicopter Fault Detection and Identification via Data-Driven Statistical Learning Methods," *AIAA Journal*, Vol. 0, (0), 0, pp. 1–16. DOI: 10.2514/1.J060353

24. Dutta, A., McKay, M., Kopsaftopoulos, F., and Gandhi, F., "Rotor Fault Detection and Identification for a Hexacopter Based on Control and State Signals via Statistical Learning Methods," Vertical Flight Society 76th Annual Forum, Online (due to COVID-19), October 2020.

25. "Mission Planner Overview," [Online; accessed 4-February-2022].

26. Söderström, T., and Stoica, P., *System Identification*, Prentice–Hall, 1989.

27. Lütkepohl, H., *New Introduction to Multiple Time Series Analysis*, Springer-Verlag Berlin, 2005.

28. Fassois, S. D., “Parametric identification of vibrating structures,” *Encyclopedia of Vibration*, edited by S. Braun, D. Ewins, and S. Rao, Academic Press, 2001, pp. 673–685.

29. Ljung, L., *System Identification: Theory for the User*, Prentice–Hall, second edition, 1999.

30. Kopsaftopoulos, F. P., and Fassois, S. D., “Scalar and Vector Time Series Methods for Vibration Based Damage Diagnosis in a Scale Aircraft Skeleton Structure ,” *Journal of Theoretical and Applied Mechanics*, Vol. 49, (4), 2011.

31. Fassois, S., and Kopsaftopoulos, F., *New Trends in Structural Health Monitoring*, Springer, January 2013, Chapter Statistical Time Series Methods for Vibration Based Structural Health Monitoring, pp. 209–264. DOI: 10.1007/978-3-7091-1390-5